

DAVS: RED EDGE AND OUTBURSTS

JING LUAN

University of California at Berkeley, Berkeley, CA 94720, US

PETER GOLDREICH

California Institute of Technology, Pasadena, CA 91125, US

Draft version December 14, 2024

ABSTRACT

As established by ground based surveys, white dwarfs with hydrogen atmospheres pulsate as they cool across the temperature range, $12500\text{ K} \gtrsim T_{\text{eff}} \gtrsim 10800\text{ K}$ (Tremblay et al. 2013).^a Known as DAVs or ZZ Ceti stars, their oscillations are attributed to overstable g-modes excited by convective driving (Brickhill 1990; Goldreich & Wu 1999). The effective temperature at the blue edge of the instability strip is slightly lower than that at which a surface convection zone appears. The temperature at the red edge is a two-decade old puzzle. Recently, *Kepler* discovered a number of cool DAVs which pulsate at higher frequencies and with much smaller photometric amplitudes than expected based on trends extrapolated from DAVs found by ground based observations. Remarkably, some of them exhibit sporadic outbursts separated by days, each lasting several hours, and releasing $\sim 10^{33} - 10^{34}\text{ erg}$ (Bell et al. 2016a). We provide quantitative explanations for both the red edge and the outbursts. The minimal frequency for overstable modes rises abruptly near the red edge. Although high frequency overstable modes exist below the red edge, their photometric amplitudes are generally too small to be detected by ground based observations. Nevertheless, these overstable parent modes can manifest themselves through nonlinear mode couplings to damped daughter modes which generate limit cycles giving rise to photometric outbursts.

1. INTRODUCTION

DAVs exhibit multi-mode oscillations. Dominant modes have periods $P \sim 2\text{ min}$ near the blue edge and $P \sim 20\text{ min}$ near the red edge. Longer-period modes show larger photometric variations and greater amplitude variability (Mukadam et al. 2006). Both features are a consequence of the criterion for overstable modes, $\omega\tau_c \gtrsim 1$, where ω is the radian frequency of a g-mode and τ_c is an effective thermal timescale at the bottom of the surface CVZ (Goldreich & Wu 1999). As a DAV cools, the bottom of its CVZ deepens, τ_c increases, and the maximum period for overstability lengthens accordingly. Amplitudes of longer-period modes appear less steady with time. This is consistent with their growth times being shorter because their mode masses are smaller. Moreover, nonlinear mode couplings are more common because the number of modes per unit frequency is larger at longer periods.

The criterion, $\omega\tau_c \gtrsim 1$, is based on analysis of modes whose propagation cavities are well detached from the bottom of the CVZ. We show that the critical $\omega\tau_c$ for over-stability increases steeply below the red edge for modes which propagate up to the bottom of the CVZ. Examples of modes with $\omega\tau_c \ll 1$ and $\omega\tau_c \gg 1$ are depicted in the propagation diagram, Figure 1, in Goldreich & Wu (1999). It takes a time, τ_c , for a flux perturbation to leak out of the photosphere. Flux perturbations injected into the bottom of the CVZ by a mode with $\omega \gg 1/\tau_c$ alternate sign many times before leaking out. Thus the

flux perturbation that emerges from the photosphere is severely diminished relative to that which enters the bottom of the CVZ. This accounts for the sudden truncation of pulsations near the red edge as seen by ground based surveys (Mukadam et al. 2006). It also explains why the cool DAVs discovered by *Kepler* pulsate at higher frequencies and exhibit much smaller photometric amplitudes than expected based on previously known DAVs.¹

Modes at sufficiently high frequencies are not even detectable by *Kepler*. But as we argue in this paper, they may reveal themselves through another channel, parametric instability due to nonlinear mode coupling (Wu & Goldreich 2001), yielding photometric outbursts (Bell et al. 2015; Hermes et al. 2015; Bell et al. 2016a,b).

Our paper is arranged as follows. Section 2 details our new criterion for overstability, which explains the red edge. Section 3 argues that parametric instability involving 3-mode couplings that lead to limit cycles quantitatively accounts for the outbursts. We summarize and discuss unresolved problems in Section 4.

2. RED EDGE

2.1. Convective Driving

A g-wave propagates where ω is below both the Brunt-Vaisala frequency, N , and the Lamb frequency, L_ℓ (e.g. Cox 1983). We denote by $z_\omega \sim \omega^2 r^2 / (g\ell(\ell+1))$ the depth where $\omega = L_\ell$, and by z_b the depth at the bottom of the surface CVZ. The upper lid of a g-mode's propagation

¹ Velocities associated with g-modes do not suffer a corresponding weakening. Horizontal velocity perturbations at the stellar limb may be detectable by spectroscopy (van Kerkwijk et al. 2000).

jingluan@berkeley.edu

^a T_{eff} at the blue and red edges depends on surface gravity which is constrained by observations to be $\log(g) \approx 8.0$.

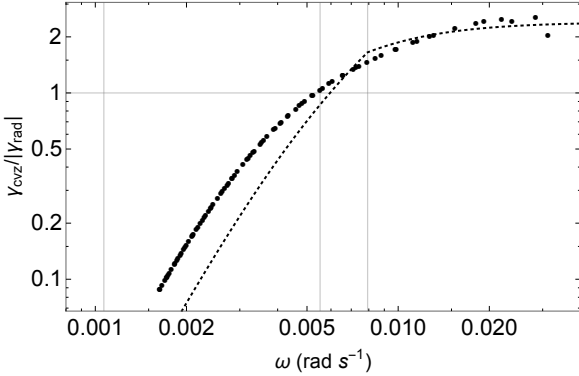


Figure 1. Filled circles show the results of quasi-adiabatic calculations, more detail of which is explained in Section 2.3. The highest radian frequency, $\approx 0.05 \text{ rad s}^{-2}$, corresponds to the dipole mode with one radial node, while the lowest frequency corresponds to the dipole mode with 90 radial nodes. The marginally overstable mode with $|\gamma_{cvz}|/|\gamma_{rad}| = 1$ has $\omega\tau_c \approx 5$. The dotted curve shows the fitting formula Equation (4).

cavity is detached from the CVZ if $z_\omega > z_b$, or equivalently, $\omega > L_{\ell,b} \equiv L_\ell(z_b)$. Otherwise the propagation cavity terminates at z_b .

Consider a g-mode with $z_\omega \gg z_b$. Upon compression of the evanescent region, heat leaks from the radiative zone into the CVZ. Thus the radiative zone contributes to damping the mode, and the CVZ contributes to its driving. According to Goldreich & Wu (1999), the ratio of convective driving to radiative damping is

$$\frac{|\gamma_{cvz}|}{|\gamma_{rad}|} \sim \frac{2(\omega\tau_c)^2}{1 + (\omega\tau_c)^2}, \quad (\omega \gg L_{\ell,b}), \quad (1)$$

leading to the criterion for over stability,

$$\omega\tau_c \gtrsim 1. \quad (2)$$

Moreover, Goldreich & Wu (1999) derive the following relation between the flux perturbation that leaks out of the photosphere and that entering the base of the CVZ;

$$\frac{\Delta F_{\text{ph}}}{F} \approx \frac{1}{1 - i\omega\tau_c} \left(\frac{\delta F}{F} \right)_{z_b}. \quad (3)$$

The criterion, $\omega\tau_c \sim 1$, for dominant modes is consistent with the observed correlation that its oscillation period lengthens with decreasing T_{eff} (Clemens 1993; Mukadam et al. 2006).

2.2. Enhanced Damping

Consider marginally overstable modes in a DAV near the red edge, $\omega\tau_c \gtrsim 1$ and $z_\omega \gtrsim z_b$. As the star cools, z_b and τ_c increase, the latter more dramatically than the former, adiabatic mode frequencies hardly change, and what were marginally overstable modes stabilize because radiative damping is enhanced relative to convective driving. Figure (1) displays the ratio of convective driving, γ_{cvz} , and radiative damping, γ_{rad} , calculated using the quasi-adiabatic technique described in Section 2.3. For comparison, the dotted curve in Figure (1) plots

$$\frac{|\gamma_{cvz}|}{|\gamma_{rad}|} \sim \frac{2.4(\omega\tau_c)^2}{1 + (\omega\tau_c)^2} \min \left[1, \left(\frac{\omega}{L_{\ell,b}} \right) \right]. \quad (4)$$

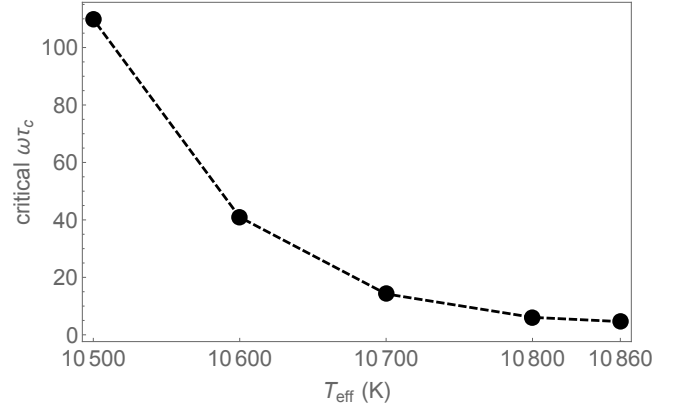


Figure 2. Critical $\omega\tau_c$ for overstable $\ell = 1$ g-modes in cool DAVs. The WD models are made using MESA. Section 2.3 details the MESA models. The critical $\omega\tau_c$ is about 5 at 10860 K, 6 at 10800 K, 14 at 10700 K, 41 at 10600 K, and 110 at 10500 K.

Convective driving at most exceeds radiative damping by a factor of ~ 2 and is easily overcome by the factor $\omega/L_{\ell,b}$.

Even below the red edge, propagation cavities of modes with sufficiently high ω remain detached from the CVZ and these modes continue to be overstable. Figure (2) plots the critical $\omega\tau_c$ for over stability below the red edge. The points are well fit by the expression

$$\omega_{\text{crit}}\tau_c \sim \exp \left[\frac{(11010 \text{ K} - T_{\text{eff}})}{110.6 \text{ K}} \right]. \quad (5)$$

Ground based surveys ‘see’ a red edge because below it, photometric amplitudes of overstable modes are too small for them to detect. Thus we now understand why the cool DAVs found by *Kepler* pulsate at higher frequencies but with much smaller photometric amplitudes than expected from DAVs discovered by ground based surveys (e.g. Bell et al. 2016a).

The smallest ω at which $z_\omega \approx \omega^2/(gk_h^2) > z_b$ is $\omega \approx \sqrt{g z_b \ell(\ell+1)/R}$. Figure (3), which plots linear damping and growth rates for modes with $\ell = 1, 2, 3$ as functions of frequency ν illustrates how the critical frequency for over stability increases with ℓ .

2.3. Work integral

MESA (Paxton et al. 2011) is employed to build a DA WD model (Paxton et al. 2011) with $M \approx 0.60 M_\odot$, $g \approx 10^8 \text{ cm s}^{-2}$, $T_{\text{eff}} \approx 10860 \text{ K}$, and hydrogen layer mass, $M_H \approx 1 \times 10^{-4} M$. The bottom of the convection zone is at pressure $p_b \approx 7.5 \times 10^8 \text{ dyn cm}^{-2}$ with $\tau_{\text{th},b} \approx 0.96 \text{ min}$ and $\tau_c \approx 15.6 \text{ min}$. Convection is treated by the ML2 version of the mixing length prescription with the mixing length parameter $\alpha = 2.0$. The atmosphere is calculated using the method by Paczyński (1969) together with the atmosphere option ‘Paczynski grey’. The first grid of the MESA model is at the optical depth ≈ 0.1 . We use MESA to evolve this WD model to lower temperatures. These cooler models are adopted to calculate the critical $\omega\tau_c$ shown in Figure 2.

GYRE (Townsend & Teitler 2013) is employed to calculate adiabatic eigenfunctions for a number of dipole g-modes. Then we calculate the work integral adopting the quasi-adiabatic technique described in Goldreich &

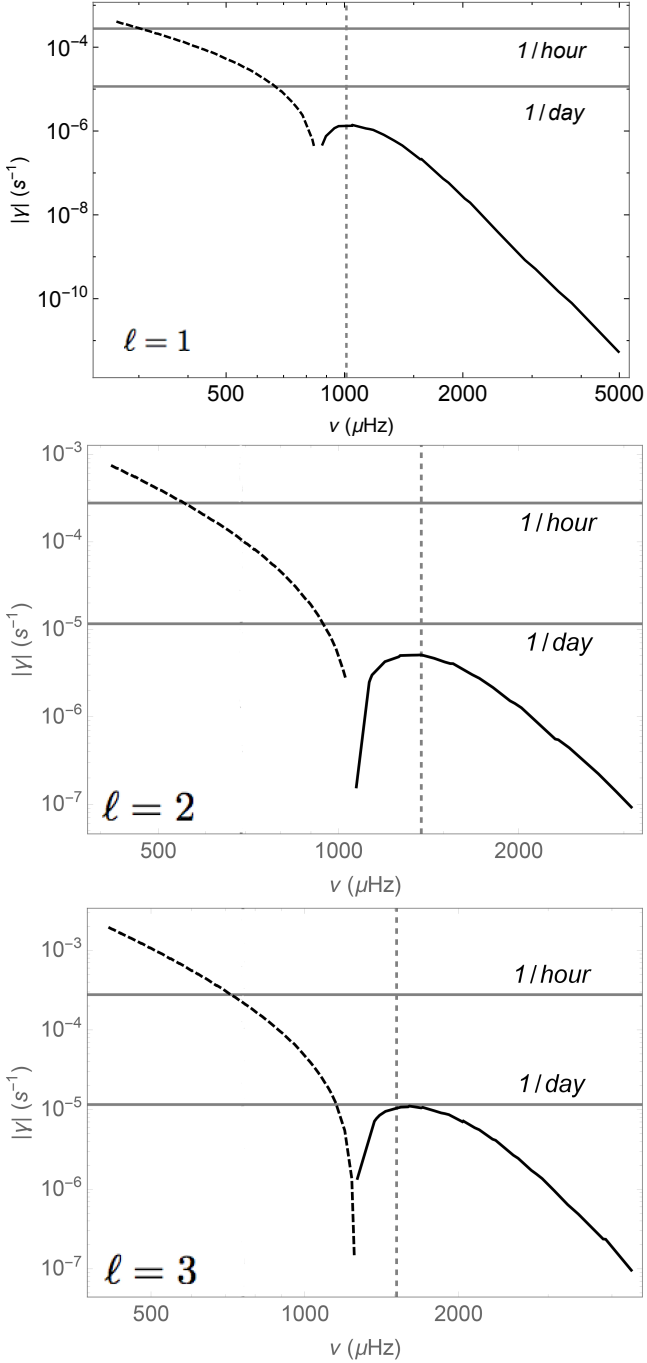


Figure 3. Linear growth and damping rates for g-modes with $\ell = 1, 2, 3$. Solid curves correspond to overstable modes with $\gamma > 0$, whereas dashed curves apply to damped modes with $\gamma < 0$. In the same WD model at $T_{\text{eff}} \approx 10860$ K, the lowest frequency of an overstable mode rises with increasing ℓ . Corresponding values of $\omega_{\text{crit}}\tau_c$ are approximately, 5 for $\ell = 1$, 6 for $\ell = 2$, and 7 for $\ell = 3$. Peak driving rates and associated frequencies, $(\gamma_{\text{pk}}, \nu_{\text{pk}}, \omega_{\text{pk}}\tau_c)$, are $(1.4 \times 10^{-6} \text{ s}^{-1}, 1048 \mu\text{Hz}, 6.2)$ at $\ell = 1$, $(5.1 \times 10^{-6} \text{ s}^{-1}, 1376 \mu\text{Hz}, 8.1)$ at $\ell = 2$, and $(1.1 \times 10^{-5} \text{ s}^{-1}, 1604 \mu\text{Hz}, 9.4)$ at $\ell = 3$. Horizontal grid lines label 1/(day) and 1/(hour). Dashed vertical lines mark the overstable mode with maximal $\gamma > 0$.

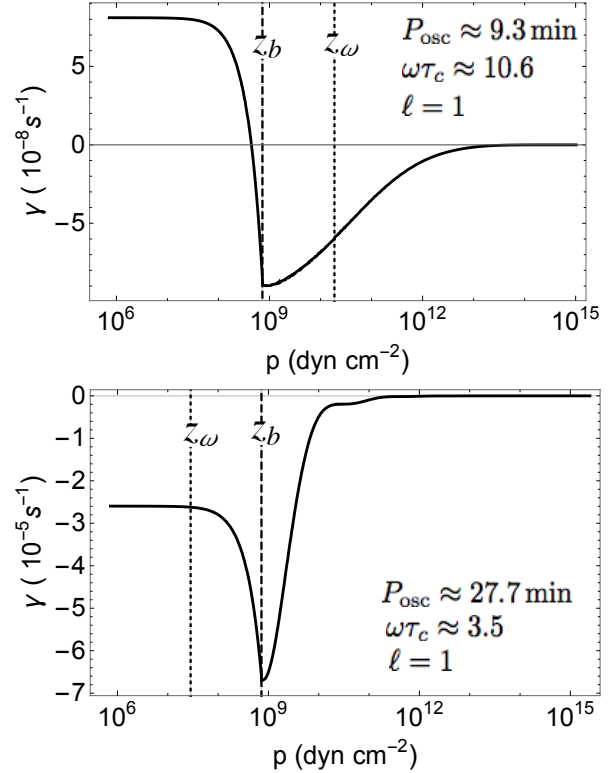


Figure 4. Work integrals for two $\ell = 1$ g-modes. The upper panel and lower panels demonstrate that the mode with $z_{\omega} \gg z_b$ is overstable, whereas the mode with $z_{\omega} \ll z_b$ is damped. Note that γ at pressure p is the net contribution to damping and driving from the region between the stellar center up to pressure p . The total damping or driving rate is given by the left end of the black solid curve in each panel. Although $\omega\tau_c \approx 3.5$ for the mode in the lower, it is damped.

Wu (1999).² Figure (4) displays $\gamma(z)$, the total driving or damping rate contributed by the region from stellar center to pressure level p , for two modes, one with $z_{\omega} \gg z_b$ and the other with $z_{\omega} \ll z_b$. The former is overstable whereas the latter is damped.

3. OUTBURSTS

Photometric outbursts from 6 cool DAVs were discovered in data collected by the Kepler satellite (Bell et al. 2015; Hermes et al. 2015; Bell et al. 2016a,b).³ Hermes et al. (2015), referring to theoretical analysis by Wu & Goldreich (2001), suggest that the outbursts may result from parametric instability. Recurring aperiodically with separations of days, individual outbursts release $\sim 10^{33} - 10^{34}$ erg and last for several hours.

Consider a parent mode resonantly coupled to two daughter modes with frequency mismatch $\delta\omega \equiv \omega_p - \omega_{d1} - \omega_{d2}$, where subscripts p , d_1 , & d_2 denote parent and daughter modes. The parent mode is overstable with linear growth rate $\gamma_p > 0$, whereas the daughter modes are damped with linear damping rates $\gamma_{d1} < 0$ and $\gamma_{d2} < 0$. Provided $|\delta\omega| < |\gamma_d|$, with $\gamma_d \equiv (\gamma_{d1} + \gamma_{d2})/2$, parametric instability results in limit cycles (Wu & Goldreich 2001). We propose that these generate photometric out-

² We normalize equation (50) in Goldreich & Wu (1999) by the total mode energy, $\omega^2 \int_0^R dr r^2 \rho (\xi_h^2 + \xi_z^2)/2 = 1$.

³ According to Hermes (private communication), the number of DAVs exhibiting outbursts currently stands at 9.

bursts. In the opposite case, $|\delta\omega| > |\gamma_d|$, parametric instability yields an equilibrium state in which the parent and daughter modes maintain constant amplitudes and the stellar luminosity is slightly elevated (Wu & Goldreich 2001). In this case, parametric instability would not generate photometric outbursts.

Individual cycles consist of three stages. In the first stage, the parent mode's energy exponentiates. The second stage begins once the parent mode's amplitude has grown sufficiently such that the rate at which energy is transferred to the daughter modes overcomes their linear damping rates and their amplitudes begin to grow. At threshold, the parent mode's energy is

$$E_{\text{th}} \sim \frac{\gamma_{d1} \gamma_{d2}}{18\kappa^2 \omega_{d1} \omega_{d2}}. \quad (6)$$

The parent mode's amplitude continues growing until its daughter modes drain its energy as fast as convective driving can replenish it. At this point, the parent mode's energy may significantly exceed E_{th} (Kumar & Goodman 1996). This initiates the third and final stage in the limit cycle during which the parent mode's amplitude undergoes a precipitous decline. After the parent mode's energy drops below threshold, the daughter modes' energies decay. The net result is the conversion of the peak energy of the parent mode to a pulse of thermal energy. An outburst arises as the pulse of thermal energy leaks through the photosphere. This completes one cycle.

The growth of the parent mode's energy in the first and second stages occurs on timescale $\sim \gamma_p^{-1}$, and may not be visible; the parent mode's propagation cavity could be deeply buried below the CVZ, i.e. $\omega_p \tau_c \gg 1$ (see equation 3), or the parent mode might have $\ell > 1$. These stages corresponds to the quiescent interval between consecutive outbursts. The third stage, conversion of the parent mode's peak energy into heat by the daughter modes lasts for $\sim \gamma_d^{-1}$. The duration of an outburst is set by the maximum of γ_d^{-1} , τ_{th} at the depth where the thermal pulse is deposited, and τ_c . The peak energy of the parent mode sets an upper limit to the energy emitted in an outburst.

As shown by Equation (12) in Wu & Goldreich (2001), magnitudes of 3-mode coupling coefficients are bounded from above by

$$|\kappa|_{\text{max}} \sim (n_p^3 L_* \tau_{\omega_p})^{-1/2}. \quad (7)$$

Here n_p is the number of radial nodes in the parent mode, L_* the stellar luminosity, and τ_{ω_p} the thermal timescale at depth z_{ω_p} . Thus the lower bound for the threshold energy is

$$E_{\text{th,min}} \sim \frac{\gamma_{d1} \gamma_{d2}}{18\omega_{d1} \omega_{d2}} n_p^3 L_* \tau_{\omega_p}. \quad (8)$$

Nonlinear effects constrain $\delta p/p < 1$ everywhere throughout the star. Since $\delta p/p$ increases outward as the background density drops, the upper bound on the parent mode's energy corresponds to $(\delta p/p)_{\text{ph}} = 1$.⁴ Figure (5) bounds the energy of prospective parent modes

⁴ In reality, it is difficult to determine the energy of the parent mode, because more descendant modes probably also participate in the energy cascade (Kumar & Goodman 1996). Arras et al. (2003) propose that energy cascades from parent mode to descendant modes in a way similar to the Kolmogorov turbulent energy

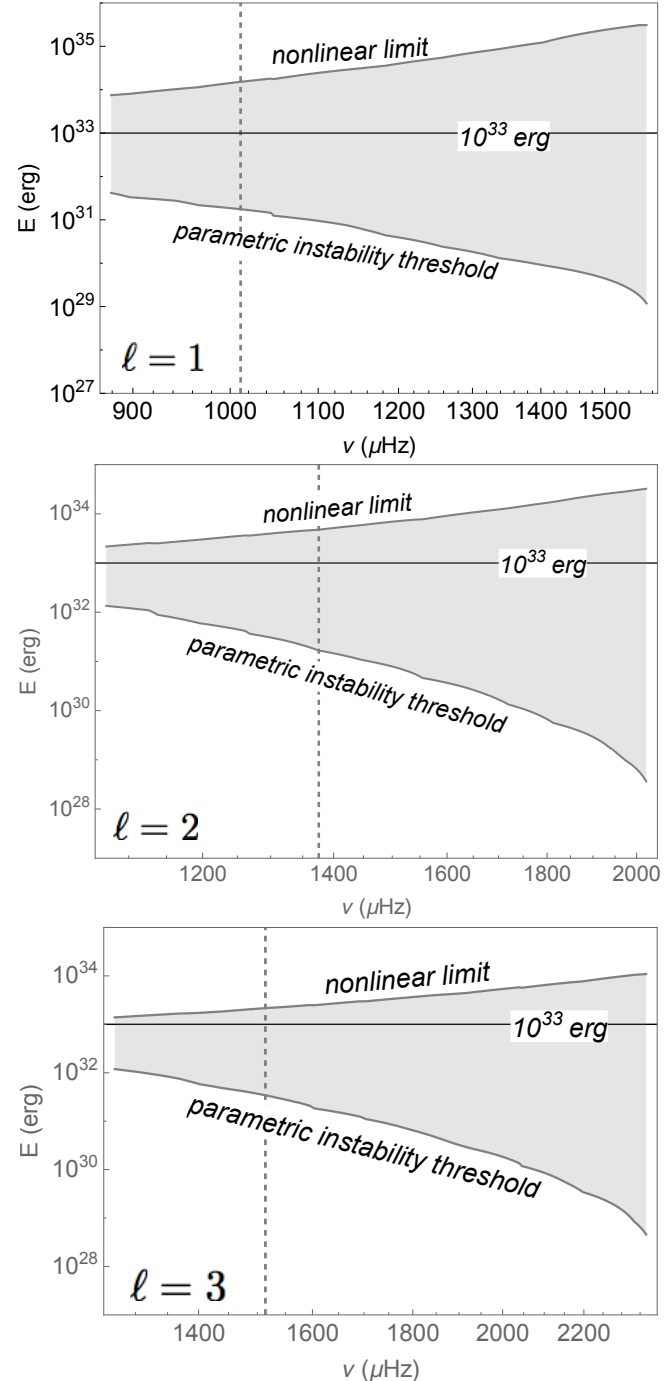


Figure 5. Energy range for prospective parent modes with $\ell = 1, 2, 3$. The vertical grid lines label the frequencies of the prospective overstability parent modes. These are the modes with maximal growth rates at each ℓ (cf. Figure (3)). Horizontal lines label the typical energy released per outburst.

between an upper limit corresponding to $(\delta p/p)_{\text{ph}} = 1$ and the lower limit $E_{\text{th,min}}$. Note that $(\delta p/p)_{\text{ph}}^2 = 1$ corresponds to $E_p \sim n \tau_{\omega_p} L_*$ (Goldreich & Wu 1999) so E_p rises with increasing ω because τ_ω grows much faster than n decreases.

Next, we examine timescales for limit cycles to assess

cascade. However, Brink et al. (2005) conclude that a small fraction of 3-mode couplings dominate the energy cascade and that the energy spectrum differs from Kolmogorov.

how they compare to recurrence rates and durations of outbursts. Figure (3) plots driving and damping rates, γ , for overstable and damped modes with $\ell = 1, 2, 3$. For each ℓ , we define ω_{pk} as the frequency at which the peak driving rate, γ_{pk} , occurs. Note that ω_{pk} is only slightly larger than the minimum frequency for an overstable mode, and also that $\omega_{\text{pk}}\tau_c$ increases slowly with ℓ , running from 6 at $\ell = 1$ through 8 at $\ell = 2$ to 9 at $\ell = 3$. More importantly, values of peak growth rates, γ_{pk} rise steeply with increasing ℓ as do the damping rates of prospective daughter modes.

We select a parent mode with $\omega \approx \omega_{\text{pk}}$ along with a matched pair of near resonant daughter modes with $\omega \approx \omega_{\text{pk}}/2$. To quantitatively account for observed outbursts, these must satisfy

$$\begin{aligned} \gamma_{\text{pk}} &\sim (\text{day})^{-1}, \\ \gamma_d &\sim (\text{hour})^{-1}, \\ \delta\omega &< \gamma_d. \end{aligned} \quad (9)$$

Horizontal lines in Figure (3) label levels at 1/day and 1/hour.

Modes with $\omega \approx \omega_{\text{pk}}$ are particularly well-suited for driving limit cycles. Radial orders of high n g-modes roughly obey⁵

$$n \propto \frac{(\ell(\ell+1))^{1/2}}{\omega}. \quad (10)$$

Thus the density of modes per unit frequency, $dn/d\omega \propto (\ell(\ell+1))^{1/2}/\omega^2$, is larger at higher ℓ and lower ω . This is beneficial for finding combinations of near resonant parent and daughter modes with $|\delta\omega| < |\gamma_d|$ that are suitable for giving rise to limit cycles and thus producing outbursts.

Choosing potential parent modes likely to be responsible for the outbursts observed by Kepler involves an interesting set of tradeoffs. The price for short limit cycles and short pulses is a smaller upper bound on peak parent mode energy. Currently, outbursts are only observed through flux increases and flux increases due to frequent short pulses may rival those from rarer long pulses although the latter have larger fluences.

Figures (6) and (7) present two examples of limit cycles involving the same $\ell = 2$ parent mode coupled to different pairs of daughter modes. In the former, the daughters are also $\ell = 2$ and the frequency mismatch, $\delta\omega \ll \gamma_d$ is even smaller than γ_p . In the latter, the daughters are identical twins with $\ell = 3$ and although $\delta\omega < \gamma_d$, it is substantially larger than γ_p . In each example, recurrence times are in excess of 10 days. The limit cycle with two quadrupole daughter modes appears chaotic, a characteristic we have observed in other cases with $|\delta\omega| < \gamma_p$. On the other hand, the limit cycle with two octupole daughter modes has $|\delta\omega| > \gamma_p$, and although not periodic, is more regular.

4. CONCLUSION AND DISCUSSION

Kepler has discovered a number of cool DAVs. They pulsate at higher frequencies and with smaller photometric amplitudes than extrapolations from DAVs found in ground-based surveys would predict. *Kepler* also detected sporadic photometric outbursts from some of these

⁵ See Figure 4 in Goldreich & Wu (1999).

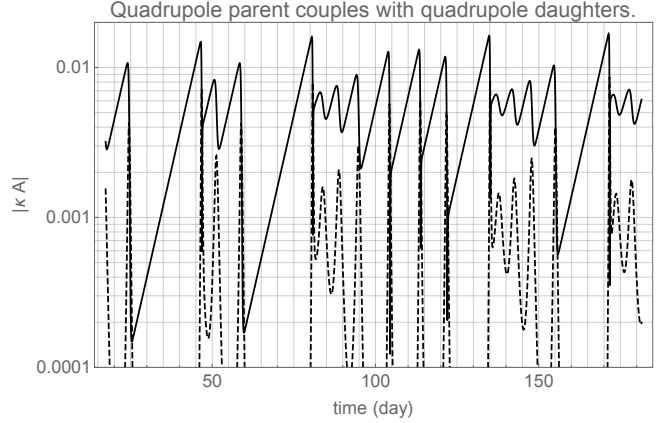


Figure 6. Plot of $|\kappa A|$ as a function of time for a limit cycle involving a quadrupole parent mode and two quadrupole daughter modes with oscillation periods $P_p \approx 12.1145$ min, $P_{d_1} \approx 23.8249$ min, and $P_{d_2} \approx 24.6537$ min. Radial orders are $n_p = 28$, $n_{d_1} = 58$ and $n_{d_2} = 59$. Rates of driving and damping are $\gamma_p \approx 5.1017 \times 10^{-6} \text{ s}^{-1}$, $\gamma_{d_1} \approx -9.6923 \times 10^{-5} \text{ s}^{-1}$, and $\gamma_{d_2} \approx -1.1678 \times 10^{-4} \text{ s}^{-1}$. The frequency mismatch, $\delta\omega \equiv \omega_p - \omega_{d_1} - \omega_{d_2} \approx 1.17736 \times 10^{-6} \text{ rad s}^{-1}$.

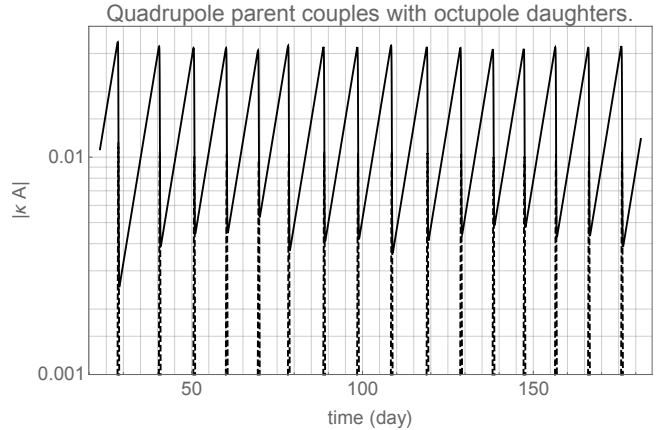


Figure 7. Plot of $|\kappa A|$ as a function of time for a limit cycle involving a quadrupole parent mode coupled to identical octupole daughter modes with oscillation periods $P_p \approx 12.1145$ min, and $P_{d_1} = P_{d_2} \approx 24.2999$ min. Radial orders are $n_p = 28$ and $n_{d_1} = n_{d_2} = 82$. Rates of driving and damping are $\gamma_p \approx 1.1082 \times 10^{-5} \text{ s}^{-1}$ and $\gamma_{d_1} = \gamma_{d_2} \approx -3.3758 \times 10^{-4} \text{ s}^{-1}$. The frequency mismatch, $\delta\omega \equiv \omega_p - \omega_{d_1} - \omega_{d_2} \approx 2.5239 \times 10^{-5} \text{ rad s}^{-1}$.

stars. These findings provide clues to both the nature of the red edge of the DAV instability strip and the action of nonlinear mode couplings in DAVs.

Modes whose propagation cavities abut the bottom of the CVZ are damped even if their frequencies satisfy $\omega\tau_c > 1$. This causes the critical $\omega\tau_c$ for overstable g-modes to rise steeply as T_{eff} decreases below the red edge. The red edge results because photometric amplitudes of modes with $\omega\tau_c \gg 1$ are too small for ground-based surveys to detect. Hopefully, sensitive photometry from space telescopes like *K2* and *TESS* will extend the DAV instability strip to even cooler stars and test whether photometric amplitudes of their oscillations continue to decline as we predict.

Heavily obscured overstable modes can reveal themselves through sporadic photometric outbursts. Three mode couplings with excellent frequency matching pro-

duce limit cycles that account for the outbursts. Thus far, outbursts have only been found in DAVs close to the red edge (Bell et al. 2016b). Relative to cool DAVs, overstable modes in hot DAVs are fewer in number, have higher frequencies, and smaller growth rates. Thus near resonant 3-mode couplings leading to limit cycles are much rarer in hot than in cool DAVs. Moreover, limit cycles in hot DAVs would have much longer recurrence times than those in cool DAVs. Thus the absence of outbursts detected from DAVs near the blue edge of the instability strip is not too surprising.

REFERENCES

Arras, P., Flanagan, E. E., Morsink, S. M., et al. 2003, *ApJ*, 591, 1129
 Bell, K. J., Hermes, J. J., Bischoff-Kim, A., et al. 2015, *ApJ*, 809, 14
 Bell, K. J., Hermes, J. J., Montgomery, M. H., et al. 2016a, ArXiv e-prints, arXiv:1609.09097
 —. 2016b, *ApJ*, 829, 82
 Brickhill, A. J. 1990, *MNRAS*, 246, 510
 Brink, J., Teukolsky, S. A., & Wasserman, I. 2005, *Phys. Rev. D*, 71, 064029
 Clemens, J. C. 1993, *Baltic Astronomy*, 2, 407
 Cox, J. P. 1983, *Theory of stellar pulsations*. (Princeton University Press)
 Goldreich, P., & Wu, Y. 1999, *ApJ*, 511, 904
 Hermes, J. J., Montgomery, M. H., Bell, K. J., et al. 2015, *ApJ*, 810, L5
 Kumar, P., & Goodman, J. 1996, *ApJ*, 466, 946
 Mukadam, A. S., Montgomery, M. H., Winget, D. E., Kepler, S. O., & Clemens, J. C. 2006, *ApJ*, 640, 956
 Paczyński, B. 1969, *AcA*, 19, 1
 Paxton, B., Bildsten, L., Dotter, A., et al. 2011, *ApJS*, 192, 3
 Townsend, R. H. D., & Teitler, S. A. 2013, *MNRAS*, 435, 3406
 Tremblay, P.-E., Ludwig, H.-G., Steffen, M., & Freytag, B. 2013, *A&A*, 559, A104
 van Kerkwijk, M. H., Clemens, J. C., & Wu, Y. 2000, *MNRAS*, 314, 209
 Wu, Y., & Goldreich, P. 2001, *ApJ*, 546, 469